KCI Concrete Journal
Vol. 13 No. 2 pp. 19-25, July 2001

Bond Analysis of Ribbed Reinforcing Bars

Oan-Chul Choi[1)]

[1)] Department of Architectural Engineering, Soong-Sil University, Korea

(Received April 20, 2001, Accepted July 23, 2001)

Abstract

A simple expression to predict bond strength of reinforcing bars with rib deformation to the surrounding is derived for the case of splitting bond failure. Finite element analysis is used to model the confining behavior of concrete cover. The roles of the interfacial properties, specifically, the friction coefficient, cohesion, the relative rib area and the rib face angle are examined.

Values of bond strength obtained using the analytical model are in good agreement with the bond test results from the previous studies.[1~3] The analytical model provides insight into interfacial bond mechanisms and the effects of the key variables on the bond strength of deformed bars to concrete. Based on the comparison between the analytical results and the test results, the values of cohesion, coefficient of friction, and the effective rib face angle are proposed.

Keywords: analytical model, bond, concrete cover, deformation of ribbed bars, finite element analysis, splitting failure

1. Introduction

Bond between reinforcing bars and concrete is provided by chemical cohesion, friction between the reinforcing bar and the surrounding matrix, and bearing against the face of the ribs. Chemical adhesion and friction play key roles in resisting initial slip of the reinforcing bar. The total bond force is the sum of the components of the bearing and friction forces on the rib acting parallel to reinforcing bar axis.

Modern reinforcing bar rib geometries date from the work by Clark[4] in 1949. Since then, the bond between concrete and deformed reinforcing bar have been investigated. Several researchers have studied the deformation characteristics of the ribbed bars to predict the ultimate strength of lapped reinforcing steel using analytical expressions.

Earlier studies have demonstrated that there is a limit to the role of the face angle of ribs measured with respect to the bar axis on the bond strength.

Lutz and Gergely[5] showed that slip of a deformed bar with a high face angle causes crushing of the concrete in front of the ribs, producing a flatter rib. They concluded that high rib face angles are flattened by crushed concrete, which reduces the effective face angle to a smaller value (Fig. 1).

The importance of the interfacial properties between steel bars and concrete, as well as bar geometries have been addressed in studies of epoxy-coated bars. Work by Choi et al.[6] has demonstrated that the lower relative bond strength of coated bars is due to the lower coefficient of friction and cohesion between concrete and epoxy-coated surfaces than obtained for uncoated surfaces.

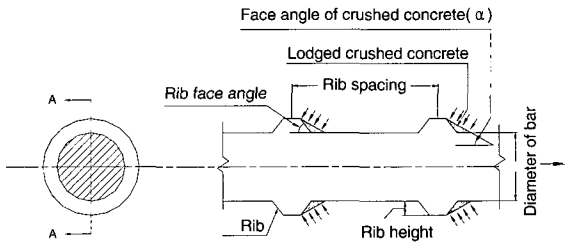

SECTION A-A

Fig. 1 Bond stress along reinforcing bar[9]

Studies by Darwin and Graham[7] demonstrated that, under relatively low confinement, bond strength is independent of deformation pattern, but under high confinement provided by transverse reinforcement or high covers, pro-

vided by transverse reinforcement or high covers, bond strength increases with an increase in the relative rib area of the bar. Idun and Darwin[8] measured average coefficients of friction between epoxy-coated and uncoated reinforcing steel and mortar of 0.49 and 0.56, respectively.

With this information as background, this study is intended to provide an overall assessment of the interfacial mechanisms that affect the bond between deformed bars and concrete. The goals of the study are to give a simple but clear picture of the bond mechanisms and to propose the realistic values of cohesion, coefficients of friction and effective rib face angles.

2. Analytical Model for Interfacial Bond Mechanisms

A splitting failure occurs in the concrete along the bar when cover or bar spacing is insufficient to resist the lateral concrete tension resulting from the wedging action of the bar deformations. As in the previous study by Cairns,[10] this wedging action makes it possible to resolve bond forces into the normal stress σ_n and the tangential shear stress τ as shown in Fig. 2. The resultant of normal components along the bar is what places the surrounding concrete in tension.

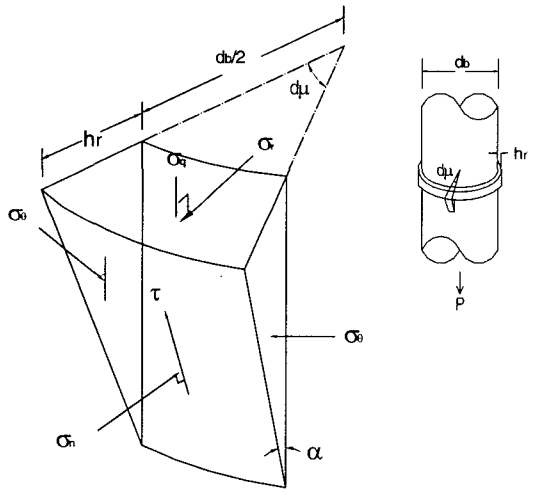

Fig. 2 Stresses acting on rib of bar[10]

Concrete under the bearing side of rib is known to be in a state of tri-axial compression with a major principal stress, the bearing stress, σ_q, on the rib acting parallel to the bar axis. Normal to the bearing stress, the minor principal stress σ_r acting radially occurs around the bar. As the radial force, the wedging force is applied to the concrete cover and confining bars, splitting occurs when the wedging force exceeds the ultimate confinement strength of the concrete cover. Bond force equal to the sum of bearing stress on the rib area along bonded length, T_1, is given by

$$T_1 = A_r \frac{l_b}{s_r} \sigma_q \tag{1}$$

in which

A_r = projected area of rib parallel to the bar axis, approximated by $A_r = \pi d_b h_r$, where h_r is rib height

$\frac{l_b}{s_r}$ = number of rib along bonded length, l_b

s_r = rib spacing

σ_q = bearing stress on bar rib acting parallel to bar axis

The frictional force between the concrete and the steel on the inclined surface of the rib may be represented using Mohr-Coulomb relation,

$$\tau = c + \mu \sigma_n \tag{2}$$

where, c = cohesion

μ = coefficient of friction

σ_n = normal stress

Suppose the stresses along the interface with an angle of α are in equilibrium with the sliding force by σ_q and the normal force by σ_r. As in Fig 3, σ_q is given by

$$\sigma_q = \sigma_r \frac{(1+\mu\cot\alpha)}{(1-\mu\tan\alpha)} + \frac{c}{\sin\alpha(\cos\alpha - \mu\sin\alpha)} \tag{3}$$

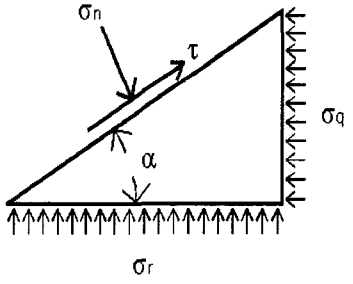

Fig. 3 Stress along interface

Eq. (3) is substituted into Eq. (1) to obtain

$$T_1 = A_r \frac{l_b}{s_r}\left[\sigma_r \frac{(1+\mu\cot\alpha)}{(1-\mu\tan\alpha)} + \frac{c}{\sin\alpha(\cos\alpha - \mu\sin\alpha)}\right] \tag{4}$$

where, σ_r acting radially around the bar axis apply to concrete cover as radial stress as shown in Fig. 4. The radial stress σ_r acts over a distance of $h_r \cot\alpha$ below the rib, and exerts a bursting force on the concrete around the bar. As in Fig. 4, the splitting failure occurs by the x component forces of the radial stresses.

Fig. 5 shows the force exerted by σ_r under one rib over a short length of the bar circumference.[10] The component of

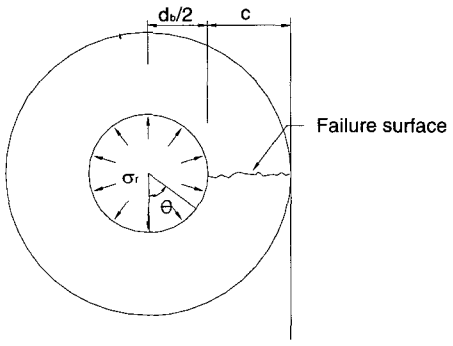

Fig. 4 Radial stress σ_r

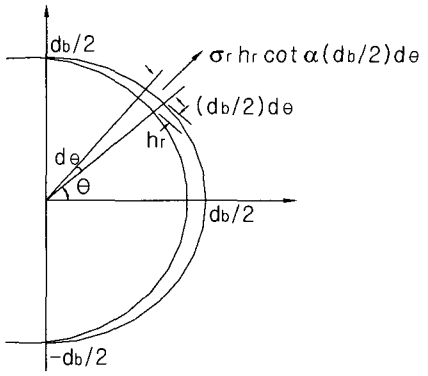

Fig. 5 Radial stress around bar circumference[10]

force in the x direction is

$$df_x = \sigma_r h_r \cot\alpha \frac{d_b}{2} d\theta \cos\theta \tag{5}$$

The resultant of σ_r on the perimeter is given by

$$f_x = \int_{-\frac{\pi}{2}}^{\frac{\pi}{2}} (\sigma_r h_r \cot\alpha)\frac{d_b}{2} d\theta \cos\theta$$

$$= \sigma_r \cot\alpha h_r d_b \tag{6}$$

Total force of σ_r on the bonded length is given by

$$F_x = \frac{l_b}{s_r} f_x = \left(\frac{l_b}{s_r}\right)(\sigma_r \cot\alpha h_r) d_b \tag{7}$$

Eq. (7) is substituted into Eq. (4) to obtain

$$T1 = Ar\frac{lb}{sr}\left(\frac{Fx}{\frac{lb}{sr}\cot\alpha hrdb}\frac{(1+\mu\cot\alpha)}{(1-\mu\tan\alpha)} + \frac{c}{\sin\alpha(\cos\alpha-\mu\sin\alpha)}\right) \tag{8}$$

In addition, the adhesion of bar surface on the bonded length may be expressed as

$$T_2 = \pi d_b l_b c \tag{9}$$

Thus, the total bond force T is given by

$$T = T_1 + T_2 \tag{10}$$

Combining with Eqs. (8), (9) and (10) results in the final equation to predict bond strength, that is expressed as follows.

$$T = F_x \pi \tan\alpha \frac{(1+\mu\cot\alpha)}{(1-\mu\tan\alpha)} + A_r \frac{l_b}{s_r}\frac{c}{\sin\alpha(\cos\alpha-\mu\sin\alpha)} + \pi d_b l_b c \tag{11}$$

The second and third terms of the right side of Eq. (11) are due to cohesion between the reinforcing bar and the concrete that is supposed to diminish increasing slip of bars

3. Finite Element Analysis

3.1 Model for Concrete Confining Force

F_x in the Eq. (11) is the confining force. It is made up of the resistance by concrete cover or by transverse reinforcement, including stirrups or ties. Resistance by cover is related to the splitting tensile strength of concrete, the magnitude of the fracture energy, and the area of failure surface.

The confining force by cover, F_x, is obtained from the finite element study to simulate surface fracture of concrete cover. The cracks observed in the bond test specimens, mainly beam-end specimens,[1] consistently reveal a splitting failure with a dominant fracture surface or running crack as shown in Fig. 6. The failure surface can be characterized as being in an opening mode where local displacements are symmetric, with the two surfaces displaced in

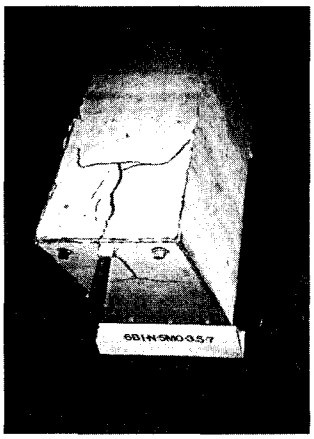

opposite directions. This basic behavior can be represented using a simple and straightforward nonlinear fracture mechanics approach.

Hillerborg et al.[11] proposed the fictitious crack model for predicting crack propagation in concrete. In a concrete specimen, it is presumed that, although the tensile strength is reached, a micro-cracked zone, the so-called fictitious crack, can transfer tensile stress. As the micro-cracks open, the tensile stress transferred across the crack decreases with increasing crack width. This stress transfer capability is represented as a stress-displacement curve,[12] illustrated in Fig. 7. As the crack width reaches w_0, all of the energy that can be absorbed by the concrete is accounted for and the tensile becomes zero. The area under this stress-displacement curve represents the energy absorbed per unit area of the crack surface in opening the crack from zero to w_0 and can be calculated as :

$$G_c = \int_0^{w_o} \sigma dw \tag{12}$$

In which, G_c is the fracture energy, σ is the tensile stress at the crack, w is the crack width, and w_0 is the displacement at which the tensile stress in the concrete becomes zero.

For the current study, the fictitious crack model is employed in the finite element analysis to represent the split

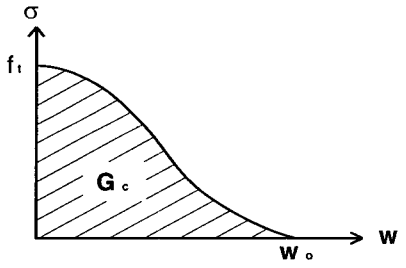

Fig. 7 Crack opening stress-displacement relationship[12]

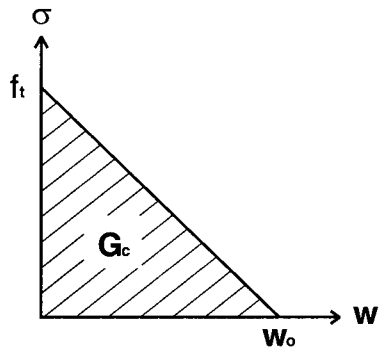

Fig. 8 Straight-line approximation of crack opening stress-displacement relationship[12]

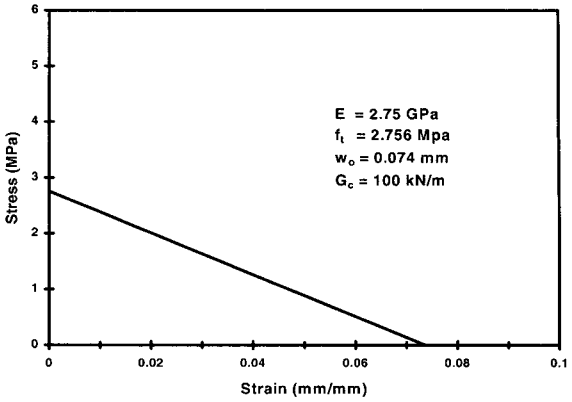

Fig. 9 Stress-strain function for rod elements[1]

ting crack that forms at the specimen centerline. The crack is represented using rod elements perpendicular to a defined fracture plane located at the specimen centerline. The elements are constrained to allow for the relative movement of nodes on either side of the crack plane perpendicular to the interface without relative movement parallel to the crack plane. The rod elements have a unit length and a total area equal to the total contact area across the crack plane.

In the initial elastic response prior to the rod elements attaining a tensile stress sufficient to begin cracking, the elements are intentionally modeled as very stiff, using a modulus of elasticity of 2.75 GPa. Upon reaching the tensile stress corresponding to the onset of tensile cracking, the rod elements are then constrained to follow a predefined stress-displacement relationship, such as illustrated in Fig. 8.[12] For the current study, the area inside this stress-displacement curve, the fracture energy is assumed to be 100 kN/m, a G_c value corresponding to the compressive strength of the concrete used in this study. The tensile strength is set at 2.75 MPa based on the 41.5 MPa compressive strength. With these values, the displacement at which the stress in the concrete becomes zero is determined by equating the area under the stress-displacement curve to the fracture energy of the concrete. This stress-displacement relationship is converted to a stress-strain function for the nonlinear material model of the rod elements, as shown in Fig. 9.

3.2 Analysis and Numerical Results

Analysis is carried out in two steps. The first step represents the splitting of the concrete, while the next step represents the interfacial action using Eq. 11. In the first step, previous finite element analysis results[1] for the beam-end specimen are used to obtain the confining force, F_x. The element model for the beam-end specimen included representations for the deformed bar, the concrete, and the split-

ting crack plane, connected by the rod element. Concrete is represented using an 8 node three-dimensional isoparametric brick element as shown in Fig. 10.

To obtain the lateral load-lateral displacement curves, loads were applied at the nodes where the reinforcing bar would be located. The lateral load-displacement curves generated with this procedure were used to define a single

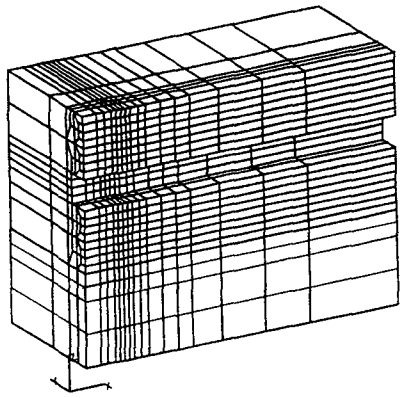

Fig. 10 FEM model for concrete substructures

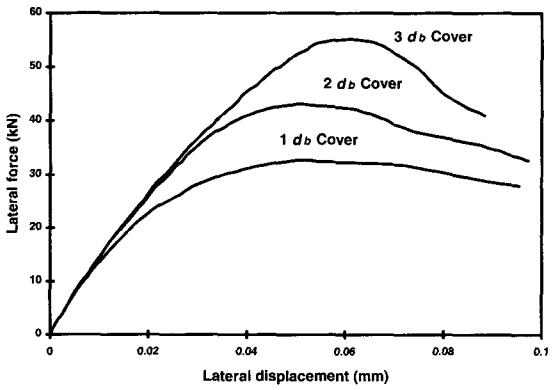

Fig. 11 Lateral load-lateral displacement curve for models with 1, 2, and bar diameter covers [1]

spring representing concrete confinement, F_x as shown in Fig. 11.

In the second step, test results for beam-end specimens with 1, 2 and 3 d_b covers are used to determine the interfacial properties such as c, μ, α. From the comparison between test and analysis results, cohesion and coefficient of friction are finally taken as 1.5 MPa and 0.45. The effective rib face angle is taken as 30 degrees, although the value appears to change depending on the magnitude of concrete cover. The procedures to determine these values are described and discussed in detail as follows.

4. Discussions

4.1 Comparison with Test Results

Bond strengths from this analysis are 173.2, 219.6 and 271.0 kN for the models with 1, 2 and 3 d_b covers, respectively, compared to average bond strengths of 142.7, 217.4 and 271.8 kN for the beam-end specimens from the experimental results[1] as in Fig. 12. The bond strength increase with additional cover is nearly linear. Bond strengths from analysis for the models with 2 and 3 d_b covers match well with those from the test results. The predicted bond

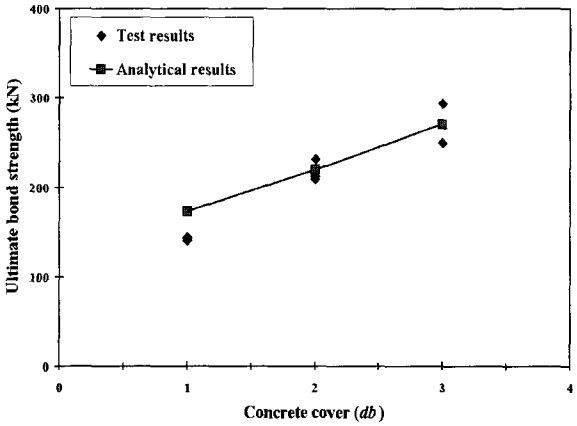

Fig. 12 Bond strength versus cover for analytical and test results with 1, 2, and 3 bar diameter covers

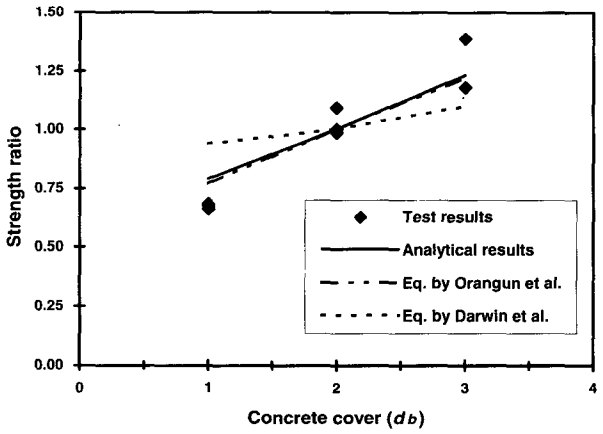

Fig. 13 Strength ratio normalized to 2 bar diameter cover versus cover: analytical results, tests results and empirical equations

strength for 1 d_b cover is higher than that of the test results.

A further comparison can be made using the empirical equations developed by Orangun, Jirsa and Breen[3] and Darwin et al..[2] For each equation, the ratios of the bond strengths obtained at 1, 2 and 3 d_b covers to the value at 2 d_b cover are compared to the analytical results in this study and the previous test results as in Fig. 13. The predicted bond strengths by Eq. (11) simply derived from the analyti-

cal models in this study agree well with those from the empirical equations in addition to the test results.

4.2 Fracture Properties of Concrete Cover

Fracture properties of the concrete cover can be evaluated by examining the results in bond strength between test data and analysis. Since the predicted bond strengths for three different covers match the test results and the empirical equations, the effect of the splitting cracking appears to be well represented by concrete fracture theory. The load-slip response for the model leading to a smooth descending branch showed much ductile compared to that of the test specimens. The match between the predicted and the test bond-slip response could become closer if non-linear approximation of fracture energy for the cover concrete were used.

From Eq. (11), it is clearly observed that concrete cover provide a confining force that is directly proportional to bond strength after cohesion lost. The simple equation with finite element model provides insight into interfacial bond mechanism ant the effects of the interfacial properties on the bond. The properties are mainly cohesion, the coefficient of friction, in addition to the effective rib face angle.

4.3 Cohesion, Coefficient of Friction, and Effective Rib Face Angle

Cohesion: The second and third terms in Eq. (11) show that the bond resistance from cohesion in function of the projected rib area and the surface area of the embedded bar. Thus the rib height or rib area affects the bond resistance until adhesion may be lost.

One way to determine the value of cohesion is to evaluate the bond test results. It is assumed that when a half of the bar diameter is embedded in concrete, only cohesion contribute the bond strength. For this virtual situation, concrete cover becomes –0.5 d_b, and then ultimate bond strength can be predicted approximately 50 kN from data fitting in Fig. 10 and the cohesion is calculated as 3.0 MPa. It is further assumed that the cohesion at half of the interface of bar is lost at ultimate load from large bond slips. Thus, the value of cohesion reduced as 1.5 MPa for concrete compressive strength of 41.5 MPa, as the cohesion may depend on strength of concrete in itself.

Coefficient of Friction: The coefficient of friction and effective rib face angle are the key variables in determining the bond strength using Eq. (11). Bond strength increases as coefficient of friction increases. Bond strength increases also as the effective rib face angle increases. Therefore, there should be upper limits for the two values. For a specific value of bond strength, a combination for the two values, coefficient of friction and the effective rib face angle can be declared with a certain ranges considering the variations. Since the coefficient of friction between concrete and concrete is reported as lower than between concrete and steel, the lower value of friction coefficient seems to be reasonable for this observation. The value of 0.45 used in this study matches well with the test data.

Effective Rib Face Angle: Slip of a reinforcing bar with respect to the concrete has the effect of crushing the concrete in front of the ribs of bar. The crushing of concrete was reported to produce the effective rib face angle of 30 to 40 degrees by Lutz and Gergely in their early study.[5] The effective rib face angle not only depends on material properties but also the structural properties. An effective rib face angle, 30 degrees, taken in this case, seems to be realistic. For more realistic values of interfacial properties, further analysis is needed.

4.4 Deformation Patterns

The first term of the right part in Eq. (11) shows that the mechanical friction component is independent of the relative rib area after the lost of cohesion. Thus, it implies that the relative rib areas have little effects on the bond strength of deformed bars when the bar is only governed by splitting bond failure. This observation closely matches with an earlier experimental study by Darwin et al.[7] that bond strength is independent of deformation patterns under relatively low confinement.

The deformation pattern, however, may affect the bond strength since the bond mechanism is affected by not only splitting failure mode but also pullout failure mode at any degree of confinement by cover or transverse reinforcement in practice. Further analytical study is needed to examine the pullout failure mode, specially the combined effects of the two different failure modes on bond strength for bars with different deformation patterns.

5. Conclusions

Following is the summary of findings in this study.

1) A simple expression to predict bond strength is derived to analyze interfacial geometry between ribbed bars and concrete.
2) The predicted bond strengths agree well with the test results and empirical equations.
3) Concrete cover provides a confinement force that is directly related to bond force after adhesion is lost. Splitting cracks of cover is well represented using the concrete fracture theory.
4) Effects of cohesion, coefficient of friction, and the effective rib face angle on bond strength are closely examined

with the analytical model.

5) The deformation pattern of bars has little effect on the bond strength of deformed steel when bond failure is only governed by the splitting mode.

References

1. Choi, O. C., Darwin, D., and McCabe, S. L., "Bond Strength of Epoxy-Coated Reinforcement to Concrete," *SM Report*, No. 25, University of Kansas Center for Research, Lawrence, Kans., July, 1990, pp. 217
2. Michael L. Tholen, and Darwin. D., "Effects of Deformation Properties on the Bond of Reinforcing Bars," University of Knasas for Research, Lawrence, Kansas, 1996, pp. 62-70.
3. Orangun, C. O., Jirsa, J. O., and Breen, J. E., "A Reevaluation of Test Data on Development Length and Splices," *Journal of the American Concrete Institute*, V. 74, No. 3, Mar., 1977, pp. 114-122.
4. Clark, A. P., "Bond of Concrete Reinforcing Bars," *Journal of American Concrete Institute*, V. 46, Nov., 1949, pp. 161-184.
5. Lutz, L. A., and Gergely, P., "Mechanics of Bond and Slip of Deformed Bars in Concrete," ACI Journal, Proceedings V. 64, No. 11, Nov., 1967, pp. 711-721.
6. Choi, O. C., Hadje-Ghaffari, H., Darwin, D., and McCabe, S. L., "Bond of Epoxy-Coated Reinforcement to Concrete: Bar Parameters," *ACI Materials Journal*, V. 88, No. 2, Mar-Apr., 1991, pp. 207-217.
7. Darwin, D., and Graham, E. K., "Effect of Deformation Height and Spacing on Bond Strength of Reinforcing Bars," *ACI Structural Journal*, V. 90, No. 6, Nov-Dec., 1993, pp. 646-657.
8. Idun, E. K., and Darwin, D., "Bond of Epoxy-Coated Reinforcement: Coefficient of Friction and Rib Face Angle," *ACI Structural Journal*, V. 96, No. 4, July-Aug., 1999, pp. 609-615.
9. Tefers, R., "Cracking of Concrete Cover along Anchored Deformed Reinforcing Bars," Magazine of Concrete Research, V. 31, No. 106, Mar., 1979, pp. 3-12.
10. Cairns, J., "An Analysis of the Ultimate Strength of Lapped Joints of Compression Reinforcement," *Magazine of Concrete Research*, V. 31, No. 106, Mar., 1979, pp. 19-27.
11. Hillerborg, A., Modeer, M., and Petersson, P.E., " Analysis of Crack Formation and Crack Growth in Concrete by Means of Fracture Mechanics and Finite Elements," *Cement and Concrete Research*, V. 6, No. 6, Nov., 1976, pp. 773-782.
12. Petersson, P. E., "Fracture Energy of Concrete: Method of Determination," *Cement and Concrete Research*, V. 10, No. 1, Jan., 1980, pp. 79-89.